ACS APPLIED ELECTRONIC MATERIALS

pubs.acs.org/acsaelm

Article

Bright Benzindolo-Benzochalcogenazolo-Based *N,N*-Coordinated Difluoroboron Complexes Exhibiting Yellow Electroluminescence Targeting White Organic Light Emitting Diodes

Published as part of ACS Applied Electronic Materials special issue "Early Career Forum 2026".

Stepan Kutsiy, Hanna M. Zinchenko, Yurii Kovtun, Yuliia Sadova, Andrii Hotynchan, Dmytro Volyniuk,* Justyna Mech-Piskorz, Pavlo Stakhira, Gonzalo Angulo, Juozas V. Grazulevicius,* and Mykhaylo A. Potopnyk*

Cite This: *ACS Appl. Electron. Mater.* 2026, 8, 5372−5383

Read Online

ACCESS | Metrics & More | Article Recommendations | Supporting Information

ABSTRACT: Three benzindolo−benzochalcogenazolo-based boron difluoride complexes (**bI-NNB-bCh**) incorporating benzoxazole, benzothiazole, and benzoselenazole acceptor units were synthesized and studied as emissive materials for organic light-emitting diodes (OLEDs). The compounds exhibit favorable electrochemical and photophysical properties, enabling their integration into vacuum-deposited OLEDs. Devices employing a conventional OLED host produce yellow−green electroluminescence with external quantum efficiencies (EQE_{max}) of 3.80%. Among the investigated emitters, the benzothiazole derivative delivers the best device performance, consistently with its higher photoluminescence quantum yield of 96% in the polymeric matrix. Replacing an OLED host exhibiting thermally activated delayed fluorescence results in near-white electroluminescence, demonstrating the critical influence of host−guest interactions and excited-state environments on emission characteristics. Under these conditions, close to 25% enhancement of EQE_{max} was achieved for the benzothiazole-based devices emitting near-white electroluminescence with color coordinates of (0.38; 0.42). These results highlight heteroaromatic acceptor engineering within the **bI-NNB-bCh** framework as an effective strategy for tuning photophysical properties and OLED performance.

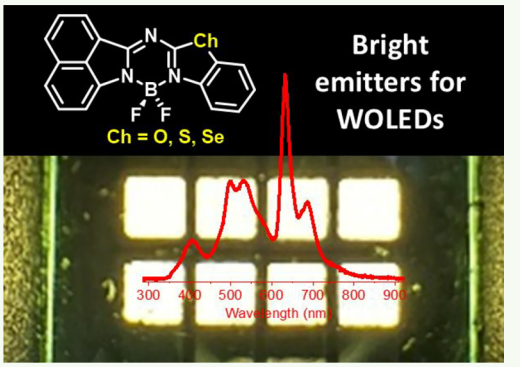

KEYWORDS: *OLED, difluoroboron dye, chalcogen, selenium, benz[c,d]indolo, electroluminescence, solid-state luminescence, optoelectronics*

INTRODUCTION

Organic light-emitting diodes (OLEDs) have turned out to be a potent innovation for next-generation display and solid-state lighting applications because of their advantages, such as low power consumption, mechanical flexibility, and the ability to produce highly saturated colors.[1−3] In particular, white OLEDs (WOLEDs) are attracting considerable attention for lighting and full-color display technologies, as they can provide high color rendering quality and tunable emission through the combination of multiple emissive components.[4] Achieving efficient and stable white emission, however, requires the development of emitters with precisely controlled photophysical properties, including high luminescence efficiency, suitable emission wavelengths, and good thermal and electrochemical stability.[5] In this context, yellow and orange emitters play a crucial role in WOLED architectures because they bridge the spectral gap between green and red components, and contribute significantly to balanced white light generation.[6]

Among various emissive materials, difluoroboron (BF_2) complexes have gained significant interest due to their outstanding optical features, including high fluorescence quantum yields, narrow emission bands, and notable structural tunability.[7] These characteristics make BF_2-based fluorophores promising candidates for electroluminescent devices,[8−11] solid-state lasers,[11−14] bioimaging[15−17] and supramolecular[18,19] applications. Structural modification of π-conjugated ligands coordinated to the *N,N*-chelated difluoroboron center can enhance molecular rigidity and conjugation, thereby suppressing nonradiative decay pathways and improving emission efficiency.[20]

Received: March 20, 2026
Revised: May 13, 2026
Accepted: June 3, 2026
Published: June 19, 2026

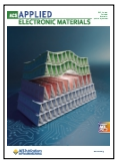

On the other hand, careful molecular design of heteroatom-containing fused aromatic systems offers unique opportunities to modulate frontier molecular orbitals, enabling fine control over absorption and emission characteristics.[11]

Fused heteroaromatic scaffolds represent promising building blocks for high-performance OLED emitters.[21] Their extended π-conjugation and planar structures favor strong light absorption and high oscillator strengths, which are essential for achieving high brightness.[22] Furthermore, the incorporation of chalcogen atoms (O, S, or Se) provides additional opportunities to fine-tune electronic properties, intermolecular interactions, and spin−orbit coupling effects, thereby influencing emission efficiency and charge-transport behavior,[23] and can be useful in the receiving WOLEDs.[24] In this context, benz[*c*,*d*]indolo-based scaffolds, when fused with benzochalcogenazole motifs, provide an extended and rigid conjugated system that can promote radiative decay while suppressing nonradiative pathways.[25,26] However, systematic studies on such fused heterocyclic ligands in *N*,*N*-coordinated difluoroboron complexes has received limited attention, particularly in the context of electroluminescent device applications.

Recently, we developed *N*,*O*-coordinated benzochalcogenazolo-based boron difluoride complexes, **Ph-ONB-bCh** (Figure 1a), which exhibit relatively high photoluminescence in the solid state.[27] However, owing to significant intramolecular rotational freedom and the resulting nonradiative deactivation of the excited dye molecules, these compounds show negligible emission in solution. Restricting intramolecular motion is essential for enhancing their emissive properties in solution and provides a clear rationale for further structural modification. Taking this into account, we decided to modify the molecular structure by exchanging benzoyl group into rigid benzo[*c*,*d*]indole unit.

Therefore, in this research, we describe the design, synthesis, and photophysical study of benzindolo-benzochalcogenazolo-based *N*,*N*-coordinated difluoroboron complexes **bI-NNB-bCh** (Figure 1b), rigidified analogues of **Ph-ONB-bCh**. The molecular architecture combines a rigid fused heteroaromatic backbone with a BF_2 coordination center to achieve a strong orange emission and high luminescence efficiency. Detailed spectroscopic and electrochemical studies reveal the influence of the chalcogen-containing framework on the electronic structure and emission behavior of the complexes. Furthermore, their electroluminescent performance was evaluated in OLEDs, demonstrating bright orange emission suitable for incorporation into warm white OLED systems. The results highlight the potential of benzindolo-benzochalcogenazolo-derived difluoroboron complexes as efficient orange emitters and provide valuable insights into the molecular design of advanced luminescent materials for high-performance WOLED applications.

■ RESULTS AND DISCUSSION

Synthesis and Characterization

Compounds **1**–**3** (Scheme 1) were obtained by a one-pot synthesis starting from benz[*c*,*d*]indol-2(1*H*)-one (**4**) and benzo[*d*]azol-2-amines **5**–**7**, using phosphoryl chloride ($POCl_3$) in hot toluene, followed by treatment with boron trifluoride etherate ($BF_3{\cdot}OEt_2$) in the presence of *N*,*N*-diisopropylethylamine (DIPEA). The starting benzo[*d*]oxazol-2-amine (**5**) and benzo[*d*]thiazol-2-amine (**6**) are commercially available, whereas benzo[*d*][1,3]selenazol-2-amine (**7**) was synthesized from 2,2′-diselanediyldianiline (**8**)[28] by treatment with hypophosphorous acid and cyanogen bromide (BrCN) in hot ethanol. The synthesized compounds were characterized by ^{1}H, ^{13}C, ^{19}F, ^{77}Se NMR spectroscopy and high-resolution mass spectrometry (HRMS).

The thermal properties of compounds **bI-NNB-bCh** were studied by thermogravimetric analysis (TGA) and differential scanning calorimetry (DSC). TGA measurements (Figure S1a,c,e in the Supporting Information) showed that boron difluoride complexes **1**, **2**, and **3** exhibit decomposition temperatures (T_d, defined as 5% weight loss) of 312, 318, and 343 °C, respectively, under a nitrogen atmosphere.

DSC analysis (Figure S1b,d,f in the Supporting Information) revealed that, during the first heating from −10 to 290 °C, compounds **1**, **2**, and **3** exhibit clear melting transitions at 281, 263, and 271 °C, respectively. Next, upon subsequent cooling from 290 to −10 °C, each compound shows a single crystallization peak at 252, 236, and 236 °C for boron difluoride complexes **1**, **2**, and **3**, respectively. During the second heating cycle, the melting temperatures remain nearly unchanged at 281, 262, and 271 °C for compounds **1**, **2**, and **3**, respectively.

Overall, the investigated compounds demonstrate high thermal stability and reproducible phase transitions, supporting their suitability for vacuum-deposited optoelectronic applications.

Quantum Chemical Calculations

To guide the interpretation of the measured photophysical properties of boron difluoride complexes **bI-NNB-bCh** quantum chemical calculations were employed. The ground state geometries were optimized at B3LYP functional with 6-31G(d) basis set employing an additional SDD method on the selenium atom. Because of the planar configuration of all synthesized fluorophores, a great extent of π-electron conjugation occurs. Consequently, the highest occupied molecular orbital (HOMO) and the lowest unoccupied molecular orbital (LUMO) take up the whole molecules (Figure 2). The introduction of heavier chalcogens such as sulfur or selenium barely influence frontier orbitals energies. Therefore, HOMO energies equal to −5.90, −5.82 and −5.83 eV whereas LUMO energies reach values of −2.62, 2.65 and 2.69 eV for dyes **1**, **2**, and **3**, respectively. Nevertheless, a slight difference in HOMO-LUMO energy gap occurs: 3.28, 3.17 and 3.14 eV, which suggests a bathochromic shift of absorption spectra in the order benzoxazole → benzothiazole → benzoselenazole derivatives. In contrast to **Ph-ONB-bCh**,[27] rigidified derivatives **bI-NNB-bCh** possess higher HOMO energies and lower values of LUMO resulting in decreasing HOMO-LUMO energy gap. These results assume bathochromic shift of absorption bands for **bI-NNB-bCh** in comparison to **Ph-ONB-bCh.**

In order to shed light on the influene of chalcogen nature on photophysical behavior of boron difluoride complexes **1**–**3** energies of singlet and triplet states, as well as spin-orbit coupling matrix elements (SOCMEs) were estimated using PBE0 functional with ZORA-DEF2-TZVP basis set and RI-SOMF(1X) function to accelerate the spin-orbit coupling (SOC) integrals in Orca 6.0 (Table S2 in the Supporting Information).

The calculations reveal that for compounds **1** and **2** SOC between the first singlet (S_1) and triplet excited states (T_1) is

https://doi.org/10.1021/acsaelm.6c00557
ACS Appl. Electron. Mater. 2026, 8, 5372−5383

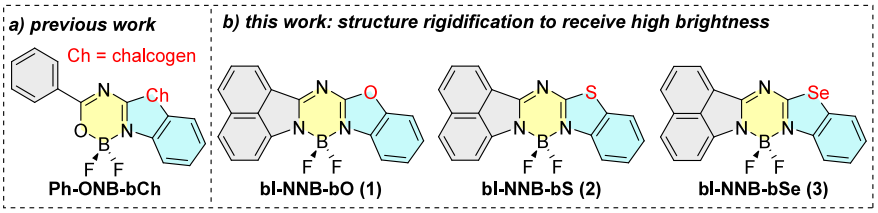

Figure 1. Benzochalcogenazolo-based boron difluoride complexes **Ph-ONB-bCh** (a) and **bI-NNB-bCh** (b).

Scheme 1. Synthesis of Boron Difluoride Complexes 1−3

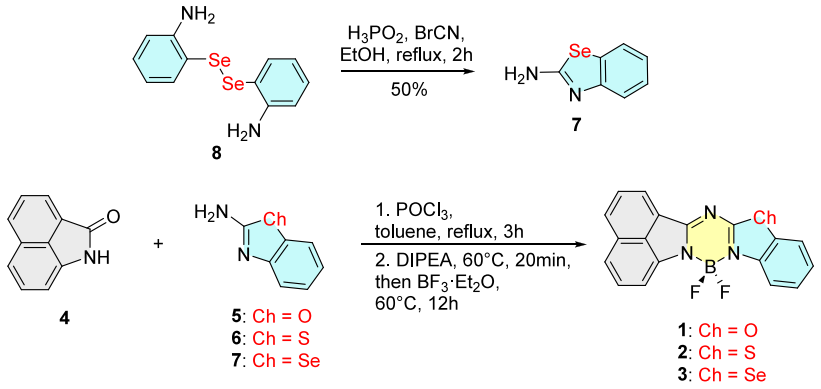

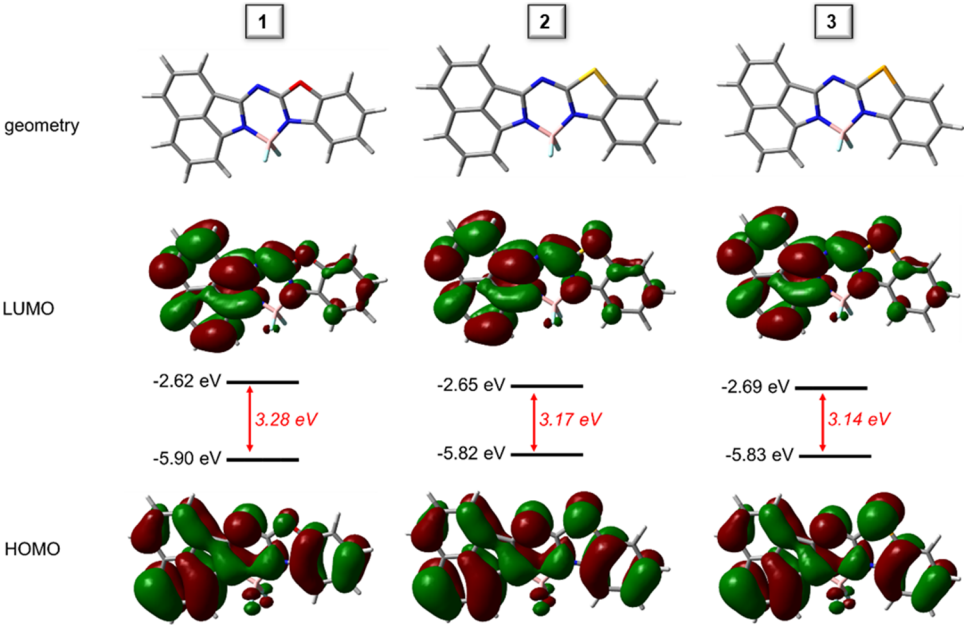

Figure 2. Optimized ground-state geometries, HOMO, and LUMO distribution for compounds **1–3**.

low with the values of 0.27 and 0.28 cm^{-1}, respectively. Whereas for selenium-containing analogue **3** this value is higher and reaches 1.03 cm^{-1}, which is consistent with the heavy atom effect. Interestingly, SOCME values for the same transition are higher for the corresponding compounds of **Ph-ONB-bCh**[27] series.

On the other hand, the energy gap between S_1 and T_1 is relatively large for thermally activated delayed fluorescence (TADF) phenomenon (1.12, 1.04 and 1.03 eV for dyes **1**, **2**, and **3**, respectively, Table S3 in the Supporting Information), hence de-excitation pathway $T_1 \rightarrow S_1$ with following $S_1 \rightarrow S_0$ could barely occur. In contrast, the energy gap between the second triplet excited state (T_2) and S_1 is significantly lower (0.12, 0.12, and 0.09 eV for compounds **1**, **2**, and **3**, respectively).

However, the corresponding SOCME values remain moderate: 1.48, 0.32, and 1.00 cm^{-1} for dyes **1**, **2**, and **3**, respectively.

https://doi.org/10.1021/acsaelm.6c00557
ACS Appl. Electron. Mater. 2026, 8, 5372−5383

These results indicate that, although the incorporation of heavier atoms is generally expected to enhance SOC and facilitate reverse intersystem crossing (RISC), this effect is not dominant in the present system.

Based on our theoretical calculations, the SOCMEs and the relevant excited-state energy alignments (including T_1 energy levels and T_2-S_1 energy gaps) do not favor efficient RISC in these compounds. In particular, relatively large singlet−triplet energy gaps and/or unfavorable energetic alignment between excited states may limit the effectiveness of the heavy-atom effect. These findings suggest that the photophysical behavior is governed more by the overall electronic structure and excited-state energetics than by the presence of heavy atoms alone.

Electrochemical Properties

The electrochemical properties of fluorophores **bI-NNB-bCh** were investigated by cyclic voltammetry (CV) (Figure S2 in the Supporting Information). The ionization potentials (IPs) and electron affinities (EAs) were estimated using the relations $IP = E^{onset}_{ox} + 4.8$ and $EA = E^{onset}_{red} + 4.8$, where E^{onset}_{ox} and E^{onset}_{red} denote the onset oxidation and reduction potentials, respectively (Table 1). The IP values follow the order benzoxazole → benzothiazole → benzoselenazole derivatives, amounting to 5.90, 5.79, and 5.73 eV, for dyes **1**, **2**, and **3**, respectively, consistent with the increase in the HOMO energy level. Conversely, the EA values decrease only slightly (3.29, 3.28, and 3.24 eV for dyes **1**, **2**, and **3**, respectively), revealing minor changes in the LUMO energy level across the series. Accordingly, the HOMO−LUMO gaps decrease along the series (E_g = 2.61, 2.51, and 2.49 eV for compounds **1**, **2**, and **3**, respectively), in agreement with the observed bathochromic shift in the absorption spectra.

Photophysical Properties

We investigated the absorption and photoluminescence (PL) properties of dyes **1–3** in dilute toluene solutions (Figure 3, Table 2). Compared with **Ph-ONB-bCh** compounds,[27] the benz[*c*,*d*]indole-containing analogues **bI-NNB-bCh** exhibit pronounced bathochromic shifts in both absorption and steady-state PL spectra. Consequently, compounds **1–3** display lowest-energy absorption bands in the blue region, which are more vibronic in shape due to the rigidified molecular structure. The benzoxazole-containing compound **1** possesses a main absorption peak at 439 nm. The benzothiazole (**2**) and benzoselenazole (**3**) counterparts show bathochromically shifted absorption maxima at 452 and 459 nm, respectively, with shoulders observed at 483 and 488 nm. TD-DFT calculations assign these main absorption bands to the $S_0 \rightarrow S_1$ electronic transition (Table S1 in the Supporting Information). The series clearly demonstrates a systematic bathochromic shift in absorption following the order: benzoxazole → benzothiazole → benzoselenazole.

The PL spectra of boron difluoride complexes **1–3** in toluene closely mirror their low-energy absorption profiles. Emission maxima are observed at 513, 527, and 533 nm for dyes **1**, **2**, and **3**, respectively (Figure 3). In sharp contrast to **Ph-ONB-bCh** compounds, which exhibit weak PL quantum yields (PLQYs) in toluene (<5%),[27] the **bI-NNB-bCh** dyes show exceptionally high PLQYs: 90, >99, and 92% for the benzoxazole, benzothiazole, and benzoselenazole derivatives, respectively (Table 2).

Table 1. Onset Oxidation and Reduction Potentials, Ionization Potentials, and Electron Affinities of Compounds 1−3

dye	E^{onset}_{ox} (V)[a]	E^{onset}_{red} (V)[b]	IP (eV)[c]	EA (eV)[d]	E_g (eV)[e]
1	1.10	-1.51	5.90	3.29	2.61
2	0.99	-1.52	5.79	3.28	2.51
3	0.93	-1.56	5.73	3.24	2.49

[a]E^{onset}_{ox} − oxidation potential. [b]E^{onset}_{red} − reduction potential. [c]IP − the ionization potential obtained from cyclic voltammetry, $IP = E^{onset}_{ox} + 4.8$. [d]EA − the electron affinity, $EA = E^{onset}_{red} + 4.8$. [e]Energy gap, E_g = IP − EA.

Time-resolved PL measurements (Figure 3b) reveal nanosecond lifetimes of 6.3, 5.7, and 5.0 ns for dyes **1**, **2**, and **3**, respectively. These correspond to very high radiative rate constants, increasing along the series benzoxazole → benzothiazole → benzoselenazole (1.45×10^8 s^{-1} → 1.74×10^8 s^{-1} → 1.84×10^8 s^{-1}). Non-radiative rate constants are approximately 1.6×10^7 s^{-1} for the benzoxazole- and benzoselenazole-containing dyes, and less than 1.8×10^6 s^{-1} for the benzothiazole derivative.

To evaluate the solvent effect on the photophysical properties, we also investigated compounds **bI-NNB-bCh** in chloroform. The absorption and emission characteristics are very similar to those observed in the corresponding toluene solutions (Figure S3, Table S4 in the Supporting Information).

To further assess the influence of the surrounding environment in the solid state, dye-doped polymer films were prepared. Poly(methyl methacrylate) (PMMA) was s chosen as the polymer matrix owing to its high optical transparency and excellent film-forming properties. To minimize intermolecular interactions between dye molecules, the measurements were carried out using thin films with a low doping concentration (the dye-to-polymer ratio was fixed at 1:99, w/w). The emission spectra of the resulting films closely resemble those recorded in toluene solution, with emission maxima at 511, 525, and 531 nm for dyes **1**, **2**, and **3**, respectively (Figure 4, Table 2). As observed in solution, the benzothiazole derivative exhibits the highest efficiency in the PMMA matrix, reaching a PLQY of 96%, whereas the benzoxazole and benzoselenazole derivatives (**1** and **3**) display PLQYs of 79–80%.

Excited-state lifetimes were also determined and follow a similar trend, decreasing from the benzoxazole-containing dye **1** (7.1 ns) to the benzoselenazole analogue **3** (5.8 ns). No long-lived emission decay components were detected for the investigated dyes (Figure S5 in the Supporting Information).

The PL properties of the solid powders of dyes **1–3** were also investigated. In the solid state, all compounds exhibit pronounced bathochromic shifts in their emission spectra compared to those observed in solution and in PMMA films. The PL maxima of corresponding boron complexes **1** and **3** are centered at 638 and 609 nm, respectively, with relatively low PLQY values of 8–10%. In contrast, benzothiazole-containing dye **2** displays a markedly red-shifted emission with λ_{em} = 699 nm, accompanied by a comparatively high PLQY of 47% (Table S5, Figure S6 in the Supporting Information). Such a substantial red shift in the solid state can be attributed to intermolecular interactions, most likely involving exciplex formation or enhanced π−π interactions between neighboring molecules. The significantly higher solid-state PLQY of benzothiazole

https://doi.org/10.1021/acsaelm.6c00557
ACS Appl. Electron. Mater. 2026, 8, 5372−5383

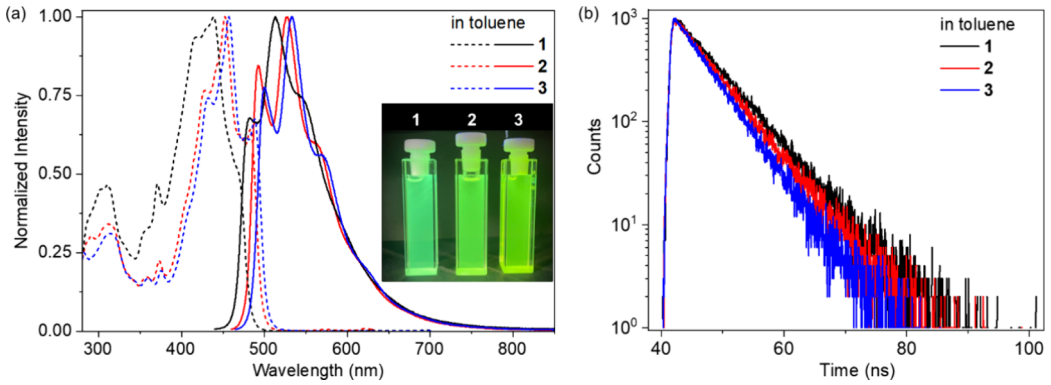

Figure 3. Normalized absorption (dashed lines) and emission (solid lines) spectra (a) and lifetime decay curves (b) of the solutions of compounds **1** (black), **2** (red), and **3** (blue) in toluene ($C = 1.0 \times 10^{-5}$ M; $\lambda_{ex} = 430$ nm). Inset: the photographs of the measured solutions taken under a 365 nm UV light illumination.

Table 2. Photoluminescence Properties of Compounds 1−3 in Toluene Solutions and the PMMA-Blended Films

dye	λ_{abs} (nm)[a]	ε (M^{-1} cm^{-1})[b]	λ_{PL} (nm)[c]	PLQY (%)[d]	τ (ns)[e]	k_r ($\times 10^8$ s^{-1})[f]	k_{nr} ($\times 10^7$ s^{-1})[g]
1	439	20,500	513/511	90/80	6.2/7.1	1.45/1.13	1.61/2.82
2	452	25,000	527/525	>99/96	5.7/6.1	>1.74/1.57	<0.18/0.66
3	457	31,500	533/531	92/79	5.0/5.8	1.84/1.36	1.60/3.62

[a]Wavelength of the absorption maximum, measured in toluene (at 298 K at $C = 2.0 \times 10^{-5}$ M). [b]Molar absorption coefficient at the maximum absorption. [c]Wavelength of the photoluminescence maximum, measured in toluene (at 298 K at $C = 2.0 \times 10^{-5}$ M)/PMMA (1 wt % of the dye). [d]Photoluminescence quantum yields in toluene/PMMA. [e]Fluorescence lifetime in toluene/PMMA. [f]Rate constant of radiative deactivation in toluene/PMMA. $k_r = \Phi/\tau$. [g]Rate constant of non-radiative deactivation in toluene/PMMA. $k_{nr} = (1 - \Phi)/\tau$.

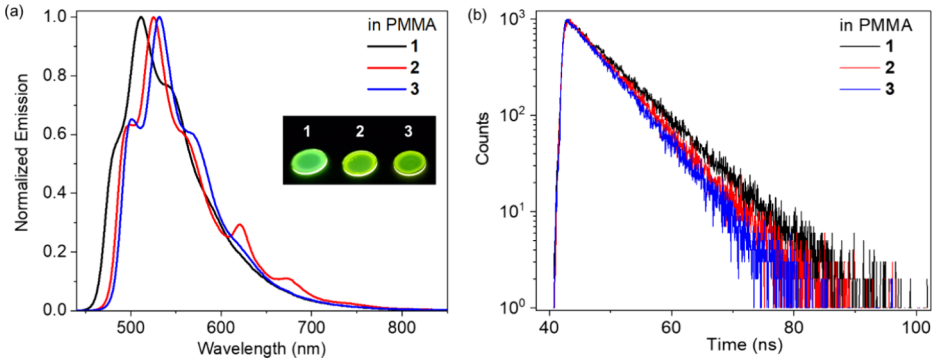

Figure 4. Normalized photoluminescence spectra (a) and lifetime decay curves (b) of the solutions of compounds **1** (black), **2** (red), and **3** (blue) in PMMA (1 wt % of the dye; $\lambda_{ex} = 430$ nm). Inset: the photographs of the measured samples taken under a 365 nm UV light illumination.

derivative **2** is likely associated with differences in molecular packing and intermolecular interactions, which can suppress non-radiative decay pathways. This behavior is consistent with trends observed for related benzochalcogenazole-based boron difluoride complexes reported in our previous studies.[11,27] The pronounced differences between the PL spectra measured in solution and in the solid state are advantageous for white-light generation, which is highly desirable for optoelectronic applications.

Electroluminescence Properties

Compounds **bI-NNB-bCh** were evaluated as emitters in OLEDs, considering their photophysical and electrochemical properties, yielding PLQYs of 96% in polymer matrix and HOMO/LUMO energy levels that enable charge injection under electrical excitation. Furthermore, the compounds exhibit greenish-yellow emissions in the polymer matrix, while their powder forms exhibit whitish emission (Figure S6 in the Supporting Information), indicating their potential for white electroluminescence. Moreover, their emission can be combined with blue emission to achieve white light generation.

In light of these attributes, the electroluminescence (EL) study was structured in two parts: (i) evaluation of the electroluminescent performance of **bI-NNB-bCh** within a conventional device architecture, and (ii) incorporation of a blue TADF host/emitter to enable the development of near-white electroluminescent devices. All devices were fabricated using a vacuum deposition method. Optimal device performance was

https://doi.org/10.1021/acsaelm.6c00557
ACS Appl. Electron. Mater. 2026, 8, 5372−5383

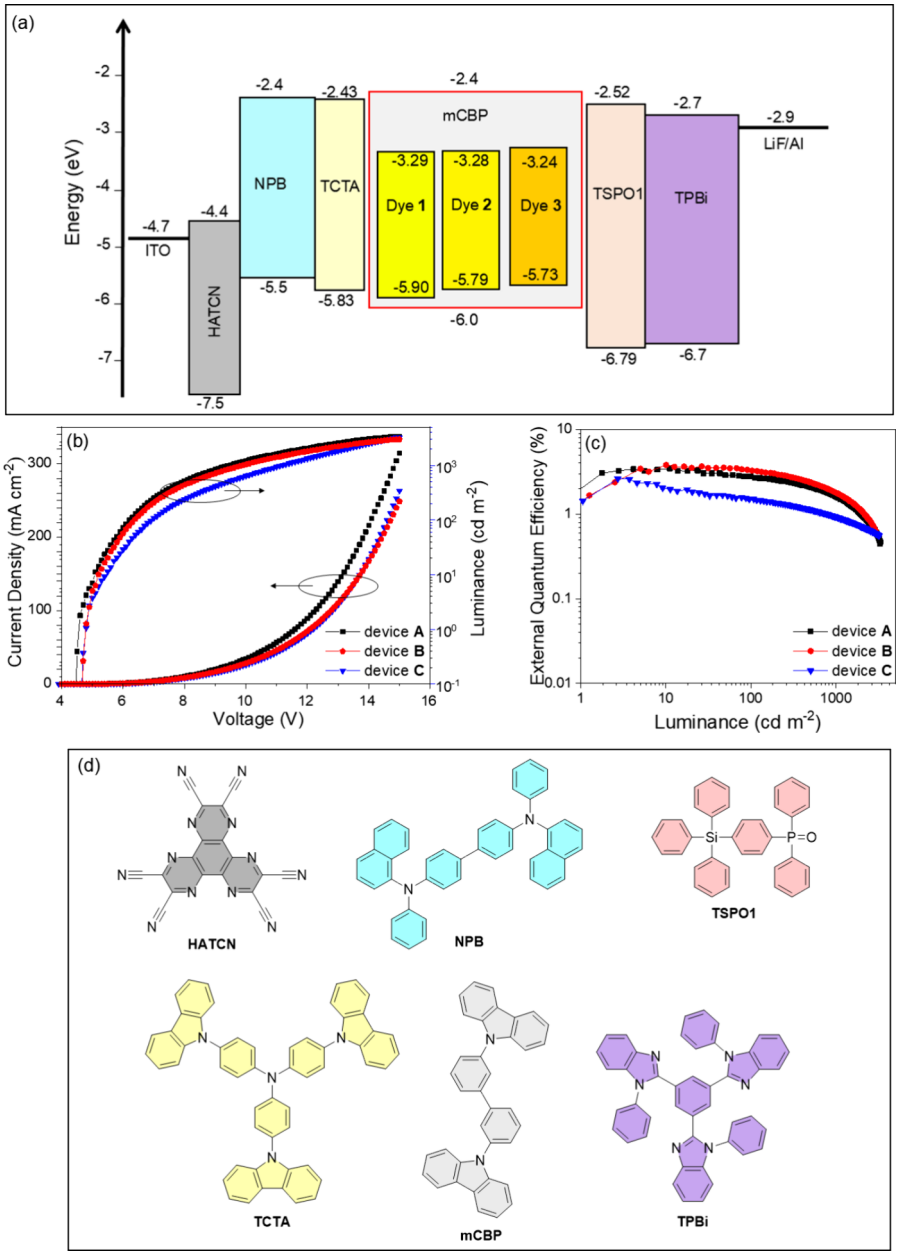

Figure 5. Electroluminescence properties of OLEDs with emitting layers of compounds **1–3** doped in mCBP (devices **A**—**C**): schematic representation of the device architecture with the energy levels (a), current density and luminance versus voltage plots (b); external quantum efficiency versus luminance (c); chemical structures of semiconductor materials (d).

achieved for emitting layers containing an emitter concentration of 10 wt %. At this concentration, improved charge transport and more efficient exciton formation within the emissive layer are likely achieved. Additionally, the higher dopant loading facilitates better energy transfer and charge balance, which are critical for enhancing electroluminescence efficiency.

First, devices employing a host—guest emitting layer with 3,3′-di(9*H*-carbazol-9-yl)–1,1′-biphenyl (mCBP) as the host were fabricated with the structure ITO/HATCN (15 nm)/NPB (40 nm)/TCTA (5 nm)/mCBP:10 wt % emitter (15 nm)/TSPO1 (5 nm)/TPBi (45 nm)/LiF (0.4 nm)/Al (120 nm) (Figure 5a). In this architecture, indium tin oxide (ITO) and Al act as the transparent anode and cathode, respectively. 1,4,5,8,9,11-Hexaazatriphenylenehexacarbonitrile (HATCN) and LiF serve as the hole- and electron-injection materials, while NPB (*N*,*N*′-di(1-naphthyl)-*N*,*N*′-diphenyl-(1,1′-biphenyl)–4,4′-diamine) functions as the hole-transport material. Tris(4-carbazoyl-9-ylphenyl)amine (TCTA) acts as an exciton- and electron-blocking material owing to its high-lying LUMO level, facilitating effective exciton confinement within the emitting layers. Diphenyl[4-(triphenylsilyl)phenyl]phosphine oxide (TSPO1) operates as a hole-blocking material due to the electron-deficient diphenylphosphine oxide moiety, whereas 2,2′,2″-(1,3,5-benzenetriyl)tris(1-phenyl-1*H*-benzimidazole) (TPBi) serves as the electron-transport material (Figure 5, Table 3). These devices exhibit turn-on voltages of 4.40 V for device **A** and 4.59 V for devices **B** and **C**, with maximum luminance values of 2984–3315 cd m^{-2}. Among them, the

https://doi.org/10.1021/acsaelm.6c00557
ACS Appl. Electron. Mater. 2026, 8, 5372−5383

Table 3. Characteristics of OLEDs A–F

device	emitter	V_{on} (V)[a]	L (cd m^{-2})[b]	CE (cd A^{-1})[c]	PE (lm W^{-1})[d]	EQE (%)[e]	CIE$_{x,y}$[f]	CIE$_{u,v}$[f]	CRI[g]	CCT[h] (K)
A	**1**	4.40	3315	8.24	5.39	3.46/2.78/1.61	(0.42; 0.54)	(0.19; 0.56)	51	3862
B	**2**	4.59	2984	7.90	4.77	3.80/3.28/1.79	(0.41; 0.54)	(0.19; 0.56)	60	3882
C	**3**	4.59	3236	6.01	3.85	2.62/1.50/0.93	(0.45; 0.51)	(0.22; 0.56)	49	3285
D	**1**	4.00	1976	5.20	3.62	3.04/2.36/1.26	(0.34; 0.43)	(0.18; 0.52)	78	4843
E	**2**	3.69	2308	6.23	4.60	4.74/3.63/2.00	(0.35; 0.41)	(0.20; 0.51)	69	4269
F	**3**	3.69	1837	7.44	5.84	3.28/2.16/1.05	(0.36; 0.47)	(0.18; 0.53)	58	4596

[a]Turn-on voltage at 1 cd m^{-2}. [b]Maximum luminance. [c] Maximum current efficiency. [d]Maximum power efficiency. [e]Maximum external quantum efficiency and EQE at 100 and 1000 cd m^{-2}. [f]Commission Internationale de l'Éclairage color coordinates CIE$_{x,y}$ (CIE1931) and CIE$_{u,v}$ (CIE1976) at 10V. [g]Color rendering indexes at 10 V. [h]Correlated color temperature at 10 V.

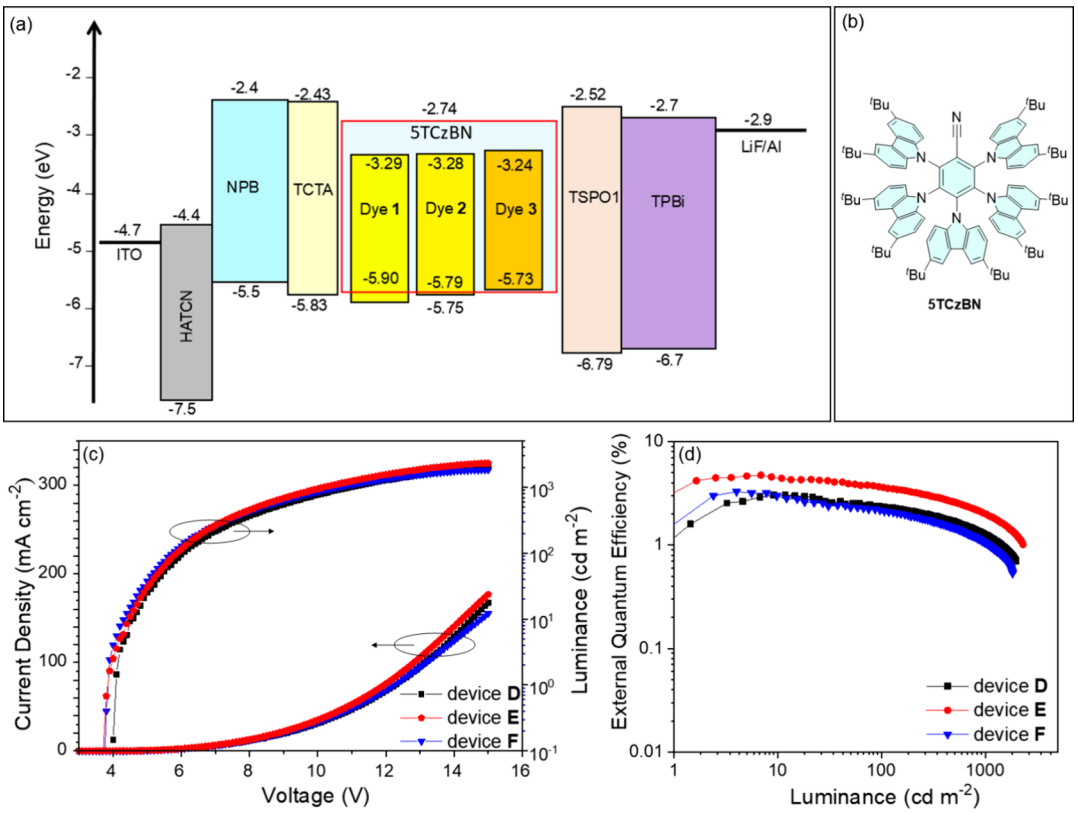

Figure 6. EL properties of near-white OLEDs with emitting layers of compounds **1**–**3** doped in 5TCzBN (devices **D**–**F**): schematic illustration of the device architecture with the corresponding energy levels (a), chemical structure of 5TCzBN (b); current density and luminance as a function of voltage (c); and external quantum efficiency as a function of luminance (d).

benzothiazole-based emitter **2** provides the highest external quantum efficiency (EQE$_{max}$) of 3.80%, while device **A**, incorporating the benzoxazole emitter **1**, achieves 3.46%. In contrast, device **C**, based on the Se-containing fluorophore **3**, shows the lowest EQE$_{max}$ (2.62%).

Second, the device architecture was further modified to either enhance EQE values or achieve near-white EL using the emitter/host 2,3,4,5,6-pentakis(3,6-di-*tert*-butyl-9H-carbazol-9-yl)benzonitrile (5TCzBN) with efficient sky-blue TADF.[29] The resulting devices had the structure ITO/HATCN (15 nm)/NPB (40 nm)/TCTA (5 nm)/5TCzBN:10 wt % emitter (25 nm)/TSPO1 (5 nm)/TPBi (45 nm)/LiF (0.4 nm)/Al (120 nm) (Figure 6). In this configuration, the benzothiazole-based emitter **2** again demonstrates the best performance, reaching an EQE$_{max}$ of 4.74% and a maximum luminance of 2308 cd m^{-2}. The enhanced EQE of device **D** is attributed to triplet harvesting via TADF in the 5TCzBN host. This is evident from the comparison of PL decay curves (Figure 7a) of the light-emitting layers **2**(10 wt %):mCBP and **2**(10 wt %):5TCzBN, corresponding to devices **B** and **D**, respectively. The **2**(10 wt %):mCBP layer exhibited a monoexponential PL decay with an emission lifetime (τ) of 4.5 ns, only slightly faster than that in toluene solution (5.7 ns). In contrast, the PL decay curve of **2**(10 wt %):5TCzBN showed a biexponential decaying behavior (τ_1 = 6.0 ns, τ_2 = 29.8 ns, Figure 7a) consistent with efficient TADF-assisted triplet harvesting. Devices **D** and **F**, incorporating emitters **1** and **3**, exhibited slightly lower efficiencies, with EQE$_{max}$ values of 3.04 and 3.28%, respectively. This trend correlates with the higher PLQY of emitter **2** relative to emitters **1** and **3**, while the heavy-atom effect associated with

https://doi.org/10.1021/acsaelm.6c00557
ACS Appl. Electron. Mater. 2026, 8, 5372–5383

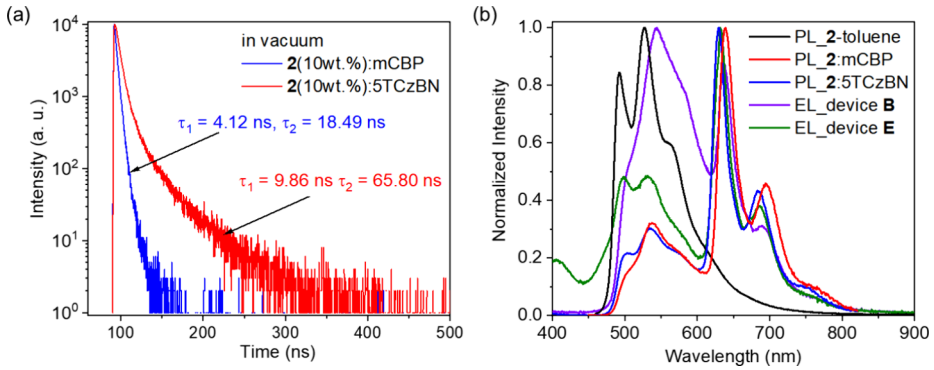

Figure 7. PL decay curves of the light-emitting layers **2**(10wt.%):mCBP and **2**(10wt.%):5TCzBN (a). Comparison of PL and EL spectra (b) of samples based on emitter **2.**

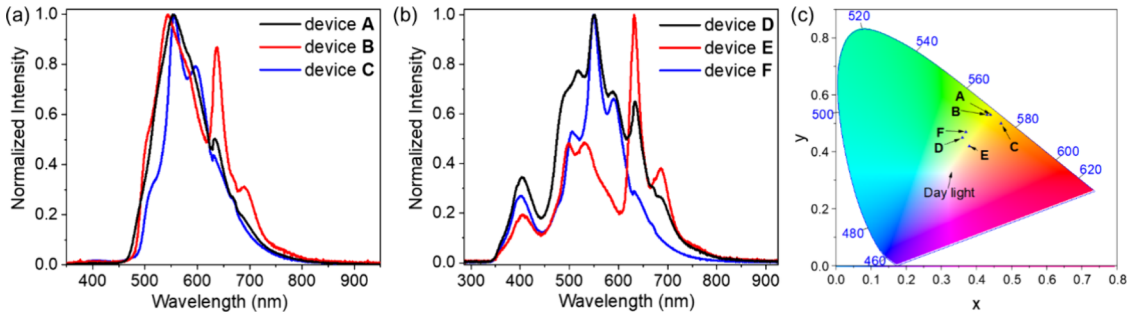

Figure 8. Electroluminescence spectra of OLEDs **A**–**C** (a) and **D**–**F** (b) at 10 V and corresponding color coordinates of devices **A**–**F** in the CIE 1931 chromaticity diagram (c).

the selenium-containing fluorophore did not significantly enhance the EL efficiency under the applied device conditions.

The yellow EL of devices **A**–**C** corresponds to the Commission Internationale de l'Éclairage ($CIE_{x,y}$ and $CIE_{u,v}$) coordinates of (x = 0.43–0.47, y = 0.50–0.53) and (u = 0.19–0.22, $v \approx 0.56$), color rendering indexes (CRI) of 49–60 and correlated color temperature (CCT) of 3285–3882 K (Table 3, Figure 6). The electroluminescence of devices **D**–**F** corresponds to CIE coordinates of (x = 0.36–0.38, y = 0.42–0.47) and (u = 0.18–0.20, v = 0.51–0.53), CRI of 58–78, and CCT of 4269–4843 K (Table 3, Figure 8c). Analysis of these color parameters indicates that device **E** exhibits warm white emission, whereas the remaining devices display near-white electroluminescence.

The EL spectra of devices **A**–**F** (Figure 8a,b) closely resemble the PL spectra of the corresponding light-emitting layers (Figure S7 in the Supporting Information). In both cases – namely, the mCBP-based devices **A**–**C** and the 5TCzBN-based devices **D**–**F** – the electroluminescence spectra exhibit vibronic structure, showing the same number of vibronic bands but with different relative intensities. No distinct bands attributable to host emission were identified, indicating efficient host–guest energy transfer within the studied emitters.

The multivibronic-band EL spectra of devices **A**–**F** are unusual and require further analysis, at least across different applied voltages (Figure S9 in the Supporting Information). Emitter **2** enabled the fabrication of devices **B** and **D**, which exhibited the highest EQE values. These devices showed consistent EL spectra across different voltages, with only minor variations in the relative intensities of the vibronic bands. The most intense narrow band, observed at 632 nm for device **D**, exhibited a full width at half-maximum (FWHM) of only 30 nm. This band was not detected in the toluene and chloroform solutions of compound **2** but was clearly visible in solid samples, such as powder, **2** (10 wt %):mCBP, **2** (10 wt %):5TCzBN, and even **2** (1 wt %):PMMA (Figures 4a, 7b, and S6 in the Supporting Information). These observations suggest that the red–near-infrared emission bands of compound **2** arise from solid-state molecular packing or crystallization, where molecular motions – including those of fluorine atoms – are fully restricted.

■ CONCLUSIONS

In conclusion, three benzindolo-benzochalcogenazolo-based boron difluoride complexes (**bI-NNB-bCh**) were prepared and their electrochemical and photophysical properties were investigated. These fluorophores incorporating benzoxazole, benzothiazole, and benzoselenazole heterocycles were evaluated as emissive materials for OLED applications. The compounds exhibit favorable photophysical and electrochemical properties, enabling their successful integration into vacuum-deposited OLED architectures. Devices employing mCBP as the host produce yellow–green electroluminescence with maximum luminance values up to 3315 cd m^{-2} and external quantum efficiencies (EQE_{max}) reaching 3.80%. Among the investigated emitters, the benzothiazole derivative consistently delivers the best device performance, which correlates with its higher photoluminescence quantum yield in the solid state.

https://doi.org/10.1021/acsaelm.6c00557
ACS Appl. Electron. Mater. 2026, 8, 5372–5383

Further modification of the device architecture through replacement of mCBP with 5TCzBN as the host enables the generation of near-white electroluminescence, highlighting the important role of host−guest interactions and excited-state environment in tuning device emission characteristics. Under these conditions, the device incorporating the benzothiazole emitter achieves the highest performance, with an EQE_{max} of 4.74% and a maximum luminance of 2308 cd m^{-2}. In contrast, incorporation of the heavier selenium atom in the benzoselenazole analogue does not lead to improved electroluminescence efficiency, indicating that the heavy-atom effect plays a limited role in the present system.

Overall, this study demonstrates that fine tuning of heteroaromatic acceptor units within the **bI-NNB-bCh** framework provides an effective strategy for modulating photophysical properties and OLED performance. The results highlight the benzothiazole motif as a particularly promising structural element for the development of efficient fluorescent emitters and underline the importance of host selection and device architecture optimization for achieving a desirable emission color and device efficiency. These findings provide useful guidelines for the future design of heterocycle-based OLED emitters.

EXPERIMENTAL SECTION

General

All reagents and chemicals (analytical grade or higher) were purchased from commercial suppliers (TCI, Acros Organics, Thermo Scientific, or Roth) and used without further purification. Synthesized compounds were purified by flash column chromatography on silica gel (Merck, 230–400 mesh). The progress of the reactions was monitored by thin-layer chromatography (TLC) using commercially available aluminum plates coated with silica gel (60 F_{254}, Merck).

Instrumental Methods

NMR spectra were recorded on a Varian Mercury 400 MHz spectrometer (400 and 375 MHz for ^{1}H and ^{19}F NMR, respectively) or a Varian VNMRS 500 MHz spectrometer (500, 125, 470, and 95 MHz for ^{1}H, ^{13}C, ^{19}F, and ^{77}Se NMR, respectively) at room temperature in $CDCl_3$. Chemical shifts were referenced to the residual solvent peak.[30] Signal multiplicities are reported as "br s", "d", "dd", "ddd", "dddd", or "m", corresponding to broad singlet, doublet, doublet of doublets, doublet of doublets of doublets, doublet of doublets of doublets of doublets, and multiplet, respectively. The data were processed using MestReNova software.

High-resolution mass spectra (HRMS) were acquired using a Synapt G2-S HDMS (Waters Inc.) mass spectrometer equipped with an atmospheric-pressure chemical ionization (APCI) source and a quadrupole time-of-flight (q-TOF) mass analyzer. Instrument control and data processing were performed using the MassLynx v4.1 software package (Waters Inc.). Spectra were recorded in APCI mode.

TGA and DSC measurements were carried out at a heating rate of 5 °C/min under nitrogen atmosphere using a TGA/DSC 3+ (Mettler Toledo apparatus) and DSC 3 (Mettler Toledo equipment), respectively.

Ground-state geometries of compounds **1–3** were optimized at the B3LYP/6-31G(d) level using Gaussian 16.[31] Main-group elements employed the 6-31G(d) basis set, while the selenium atom was additionally treated with the SDD (Stuttgart/Dresden) effective core potential,[32] which includes relativistic effects. This B3LYP/6-31G(d)/SDD approach has been extensively validated for heavy-atom systems.[33] Molecular orbitals were visualized using GaussView 6.0.[34] Spin-orbit coupling matrix elements as well as energies of singlet and triplet states were calculated using PBE0 method with ZORA-DEF2-TZVP basis set and RI-SOMF(1X) function to accelerate the spin-orbit coupling integrals in Orca 6.0.

Cyclic voltammetry measurements were performed at room temperature using a Bio-Logic SAS SP-200 potentiostat. Solutions of the studied compounds were prepared in dry acetonitrile containing tetrabutylammonium hexafluorophosphate as the supporting electrolyte. Experiments were conducted in a three-electrode setup comprising an Ag/AgCl reference electrode, a glassy carbon working electrode, and a platinum wire auxiliary electrode, with ferrocene (Fc) added as an internal standard. Voltammograms were recorded at a scan rate of 50 mV s^{-1}. All potentials are referenced to the Fc/Fc^{+} redox couple.

UV−vis absorption spectra of the solutions were recorded at room temperature using a Shimadzu UV-3600i Plus spectrophotometer. Steady-state fluorescence emission spectra were measured on an Edinburgh Instruments FS5 spectrophotometer (Edinburgh, UK) with a xenon lamp as the excitation source. Absolute fluorescence quantum yields were determined using a calibrated SC-30 integrating sphere, with excitation at the appropriate absorption wavelength for each sample. Photoluminescence decay curves of both solution and PMMA films were acquired using a pulsed diode laser (PDL 820, PicoQuant, λ_{ex} = 374 nm) in conjunction with a time-correlated single-photon counting (TCSPC) technique. All measurements were conducted at room temperature.

OLEDs

Devices were fabricated by vacuum deposition at pressures below 2 × 10^{-6} mbar using a Kurt J. Lesker system integrated into an MBraun MB EcoVap4G glovebox. Pre-patterned ITO-coated glass substrates (Ossila; sheet resistance 20 Ω sq^{-1}; eight pixels of 4.5 mm^2 each) were used. The substrates were sequentially cleaned by ultrasonication in Hellmanex solution, deionized water, and isopropanol, followed by drying under a stream of argon after each step. Subsequently, they were treated with UV−ozone for 30 min (Ossila cleaner), inspected under UV light, and immediately transferred to the glovebox.

The deposition system was equipped with two organic and two metal sources, as well as quartz crystal microbalance sensors connected to an SQC-310C controller, calibrated using a Profilm3D profilometer. This configuration enabled simultaneous control of deposition rates from two sources, allowing the formation of host−guest layers with approximately 10 wt % dopant via co-evaporation. Film and device thicknesses were verified using the profilometer. Current density−voltage (J−V) and luminance−voltage (L−V) characteristics were measured using an HP4145A semiconductor parameter analyzer. Luminance was measured with a calibrated photodiode, and EL spectra were recorded using an Ocean Optics USB2000 spectrometer. Device efficiencies were calculated from the measured luminance, current density, and EL spectra. CIE 1931 and CIE 1976 coordinates were determined using software for an Edinburgh Instruments FLS980 spectrophotometer. Correlated color temperature (CCT) and color rendering index (CRI) values were calculated using an online calculator (Waveform Lighting, https://www.waveformlighting.com/tech/color-rendering-index-calculator; accessed April 28, 2026).

Synthesis

Benzo[*d*][1,3]selenazol-2-amine (7). To a stirred solution of 2,2'-diselanediyldianiline (**8**, 350 mg, 1.02 mmol) and hypophosphorous acid (50% aqueous solution, 224 μL, 2.05 mmol) in ethanol (10 mL), cyanogen bromide (325 mg, 3.07 mmol) was added slowly at room temperature. The reaction mixture was heated at 80 °C for 2 h. The progress of the reaction was monitored by TLC. During this time, the starting material was completely consumed. Next, the reaction mixture was concentrated under reduced pressure, and the residue was treated with saturated aqueous sodium bicarbonate solution to adjust the pH to 8. The mixture was extracted with DCM (3 × 20 mL), and the combined organic layers were dried over Na_2SO_4. The solvent was removed in vacuo, and the residue was recrystallized

https://doi.org/10.1021/acsaelm.6c00557
ACS Appl. Electron. Mater. 2026, 8, 5372−5383

from isopropanol to afford amine **7** (201 mg, 50%). ^{1}H NMR (500 MHz, $CDCl_3$): δ = 7.62 (1H, dd, *J* = 7.9 Hz, *J* = 0.8 Hz, Ar−H), 7.54 (1H, dd, *J* = 8.0 Hz, *J* = 0.7 Hz, Ar−H), 7.30 (1H, ddd, *J* = 8.5 Hz, *J* = 8.2 Hz, *J* = 1.2 Hz, Ar−H), 7.06 (1H, ddd, *J* = 8.6 Hz, *J* = 7.9 Hz, *J* = 1.2 Hz, Ar−H), 5.67 (2H, br. s, NH_2) ppm; ^{13}C NMR (125 MHz, $CDCl_3$): δ = 166.09, 153.73, 134.81, 126.40, 124.43, 122.65, 120.58 ppm; ^{77}Se NMR (95 MHz, $CDCl_3$): δ = 525.67 ppm. HRMS (APCI) calcd for $C_7H_7N_2Se$ $[M + H]^+$: 198.9774, found: 198.9777.

General Procedure for Synthesis of Dyes 1−3. Compounds **1−3** were prepared using a modified literature procedure.[25] A mixture of benz[*c*,*d*]indol-2(1*H*)-one (**4**, 200 mg, 1.18 mmol, 1 equiv), the corresponding benzo[*d*]azol-2-amine **5−7** (2.36 mmol, 2 equiv), and phosphoryl chloride (0.6 mL, 6.50 mmol, 5.5 equiv) in toluene (10 mL) was refluxed for 3 h, during which time the benz[*c*,*d*]indol-2(1*H*)-one spot disappeared on TLC. After cooling to 40 °C, *N*,*N*-diisopropylethylamine (2.0 mL, 11.82 mmol, 10 equiv) was added, and the mixture was stirred at 40 °C for 20 min. Then, boron trifluoride etherate (2.0 mL, 16.55 mmol, 14 equiv) was then added, and the reaction mixture was stirred at 60 °C for 12 h. After cooling to room temperature, water (50 mL) was added, and the mixture was extracted with DCM (3 × 40 mL). The combined organic layers were dried over Na_2SO_4, filtered, and concentrated under reduced pressure. The crude product was purified by flash column chromatography on silica gel using hexanes/DCM (100:0 to 50:50, v/v) as the eluent.

8,8-Difluoro-8*H*-8λ^4,9λ^4-benzo[*cd*]benzo[4′,5′]oxazolo[3′,2′:1,6][1,3,5,2]triazaborinino[3,4-*a*]indole (1). was obtained in 32% yield (127 mg) from amine **5** (317 mg) as the starting material, following general procedure. ^{1}H NMR (400 MHz, $CDCl_3$): δ = 8.40 (1H, d, *J* = 7.1 Hz, Ar−H), 8.21 (1H, d, *J* = 8.0 Hz, Ar−H), 7.87−7.74 (4H, m, Ar−H), 7.66 (1H, dd, *J* = 8.3 Hz, *J* = 7.2 Hz, Ar−H), 7.57 (1H, dd, *J* = 8.7 Hz, *J* = 7.5 Hz, Ar−H), 7.47 (1H, dd, *J* = 8.9 Hz, *J* = 7.6 Hz, Ar−H), 7.42 (1H, dd, *J* = 8.8 Hz, *J* = 7.7 Hz, Ar−H) ppm; ^{13}C NMR (125 MHz, $CDCl_3$): δ = 165.77, 162.79, 146.73, 139.56, 133.39, 131.05, 129.61, 129.55, 129.31, 128.99, 127.40, 126.47, 126.29, 125.70, 124.21, 115.19, 115.09, 111.29 ppm; ^{19}F NMR (375 MHz, $CDCl_3$): δ = −140.90 (2H, dd, *J* = 51.5 Hz, *J* = 25.6 Hz, BF_2) ppm. HRMS (APCI) calcd for $C_{18}H_{10}BN_3O F_2$ $[M]^-$: 333.0885, found: 333.0888.

8,8-Difluoro-8*H*-8λ^4,9λ^4-benzo[*cd*]benzo[4′,5′]thiazolo[3′,2′:1,6][1,3,5,2]triazaborinino[3,4-*a*]indole (2). was obtained in 41% yield (170 mg) from amine **6** (355 nm) as the starting material, following general procedure. ^{1}H NMR (500 MHz, $CDCl_3$): δ = 8.34 (1H, d, *J* = 7.2 Hz, Ar−H), 8.17 (2H, dd, *J* = 7.9 Hz, *J* = 6.8 Hz, Ar−H), 7.82 (1H, dd, *J* = 7.8 Hz, *J* = 7.5 Hz, Ar−H), 7.80−7.72 (3H, m, Ar−H), 7.66 (1H, dd, *J* = 8.1 Hz, *J* = 7.5 Hz, Ar−H), 7.58 (1H, dd, *J* = 8.3 Hz, *J* = 7.5 Hz, Ar−H), 7.43 (1H, dd, *J* = 7.9 Hz, *J* = 7.5 Hz, Ar−H) ppm; ^{13}C NMR (125 MHz, $CDCl_3$): δ = 172.86, 162.26, 141.09, 139.81, 132.88, 129.65 (2C), 129.24, 129.01, 127.99, 127.46, 126.83, 126.54, 125.76, 123.84, 122.12, 118.54, 114.63 ppm; ^{19}F NMR (375 MHz, $CDCl_3$): δ = −139.87 (2H, dd, *J* = 57.6 Hz, *J* = 28.7 Hz, BF_2) ppm. HRMS (APCI) calcd for $C_{18}H_{10}BN_3F_2S$ $[M]^-$: 349.0657, found: 349.0664.

8,8-Difluoro-8*H*-8λ^4,9λ^4-benzo[*cd*]benzo[4′,5′][1,3]selenazolo[3′,2′:1,6][1,3,5,2]triazaborinino[3,4-*a*]indole (3). was obtained in 18% yield (83 mg) from amine **7** (466 mg) as the starting material, following general procedure. ^{1}H NMR (500 MHz, $CDCl_3$): δ = 8.35 (1H, d, *J* = 7.1 Hz, Ar−H), 8.24 (1H, dd, *J* = 8.3 Hz, *J* = 8.0 Hz, Ar−H), 8.19 (1H, d, *J* = 8.0 Hz, Ar−H), 7.85−7.73 (4H, m, Ar−H), 7.66 (1H, dd, *J* = 8.1 Hz, *J* = 7.6 Hz, Ar−H), 7.56 (1H, dd, *J* = 8.3 Hz, *J* = 0.9 Hz, Ar−H), 7.36 (1H, dd, *J* = 8.1 Hz, *J* = 0.8 Hz, Ar−H) ppm; ^{13}C NMR (125 MHz, $CDCl_3$): δ = 176.84, 160.83, 142.70, 139.77, 132.96, 129.69, 129.66, 129.29, 128.87, 127.90, 126.98, 126.47, 125.73, 125.14, 124.00, 120.25, 120.22, 120.19, 114.92 ppm; ^{19}F NMR (470 MHz, $CDCl_3$): δ = −139.14 (2H, dd, *J* = 59.3 Hz, *J* = 29.4 Hz, BF_2); ^{77}Se NMR (95 MHz, $CDCl_3$): δ = 521.07 ppm. HRMS (APCI) calcd for $C_{18}H_{10}BN_3F_2Se$ $[M]^-$: 397.0101, found: 397.0109.

■ ASSOCIATED CONTENT

Supporting Information

The Supporting Information is available free of charge at https://pubs.acs.org/doi/10.1021/acsaelm.6c00557.

(TD)DFT calculations data; additional photophysical spectra and data; and NMR spectra of the synthesized compounds (PDF)

■ AUTHOR INFORMATION

Corresponding Authors

Dmytro Volyniuk – *Department of Polymer Chemistry and Technology, Kaunas University of Technology, Barsausko 59, Kaunas LT-51423, Lithuania;* Email: dmytro.volyniuk@ktu.lt

Juozas V. Grazulevicius – *Department of Polymer Chemistry and Technology, Kaunas University of Technology, Barsausko 59, Kaunas LT-51423, Lithuania;* orcid.org/0000-0002-4408-9727; Email: juozas.grazulevicius@ktu.lt

Mykhaylo A. Potopnyk – *Institute of Organic Chemistry, Polish Academy of Sciences, Kasprzaka 44/52, Warsaw 01-224, Poland; Department of Organic Chemistry, Faculty of Chemistry, Ivan Franko National University of Lviv, Kyryla and Mefodiya 6, Lviv 79005, Ukraine;* orcid.org/0000-0002-4543-2785; Email: potopnyk@gmail.com; mykhaylo.potopnyk@icho.edu.pl

Authors

Stepan Kutsiy – *Institute of Organic Chemistry, Polish Academy of Sciences, Kasprzaka 44/52, Warsaw 01-224, Poland; Department of Electronic Engineering, Lviv Polytechnic National University, Sviatoho Yura sq. 1, Lviv 79013, Ukraine*

Hanna M. Zinchenko – *Institute of Organic Chemistry, Polish Academy of Sciences, Kasprzaka 44/52, Warsaw 01-224, Poland; Department of Organic Chemistry, Faculty of Chemistry, Ivan Franko National University of Lviv, Kyryla and Mefodiya 6, Lviv 79005, Ukraine;* orcid.org/0000-0001-5157-5339

Yurii Kovtun – *Institute of Organic Chemistry, Polish Academy of Sciences, Kasprzaka 44/52, Warsaw 01-224, Poland; Institute of Organic Chemistry, National Academy of Sciences of Ukraine, Akademika Kuharya Str. 5, Kyiv 02000, Ukraine*

Yuliia Sadova – *Institute of Organic Chemistry, Polish Academy of Sciences, Kasprzaka 44/52, Warsaw 01-224, Poland; V. Bakul Institute for Superhard Materials, National Academy of Sciences of Ukraine, Avtozavodska 2, Kyiv 04074, Ukraine;* orcid.org/0009-0009-3818-6473

Andrii Hotynchan – *Department of Organic Chemistry, Faculty of Chemistry, Ivan Franko National University of Lviv, Kyryla and Mefodiya 6, Lviv 79005, Ukraine*

Justyna Mech-Piskorz – *Institute of Physical Chemistry, Polish Academy of Sciences, Kasprzaka 44/52, Warsaw 01-224, Poland;* orcid.org/0000-0002-4778-7918

Pavlo Stakhira – *Department of Electronic Engineering, Lviv Polytechnic National University, Sviatoho Yura sq. 1, Lviv 79013, Ukraine*

Gonzalo Angulo – *Institute of Physical Chemistry, Polish Academy of Sciences, Kasprzaka 44/52, Warsaw 01-224, Poland;* orcid.org/0000-0002-6484-1795

Complete contact information is available at: https://pubs.acs.org/doi/10.1021/acsaelm.6c00557

https://doi.org/10.1021/acsaelm.6c00557
ACS Appl. Electron. Mater. 2026, 8, 5372−5383

Author Contributions

CRediT: **Mykhaylo A. Potopnyk** designed the compounds. **Hanna M. Zinchenko** and **Yurii Kovtun** performed the synthesis. **Hanna M. Zinchenko** characterized the compounds. **Stepan Kutsiy** performed the electrochemical investigation. **Andrii Hotynchan** carried out the theoretical calculations. **Stepan Kutsiy**, **Yuliia Sadova**, **Dmytro Volyniuk**, and **Justyna Mech-Piskorz** performed the photophysical characterization. **Stepan Kutsiy**, **Dmytro Volyniuk**, and **Pavlo Stakhira** fabricated the OLEDs. **Mykhaylo A. Potopnyk**, **Stepan Kutsiy**, **Andrii Hotynchan**, and **Hanna M. Zinchenko** wrote the original draft. **Dmytro Volyniuk**, **Gonzalo Angulo**, **Juozas V. Grazulevicius**, and **Mykhaylo A. Potopnyk** revised the draft. **Mykhaylo A. Potopnyk**, **Pavlo Stakhira**, **Gonzalo Angulo**, and **Juozas V. Grazulevicius** initiated, coordinated, and supervised the research and were responsible for funding acquisition. All authors contributed to discussions, reviewed and edited the manuscript, and approved the final version.

Notes

The authors declare no competing financial interest.

■ ACKNOWLEDGMENTS

S.K., H.M.Z., Y.K., and M.A.P. thank "Long-term program of support of the Ukrainian research teams at the Polish Academy of Sciences carried out in collaboration with the U.S. National Academy of Sciences with the financial support of external partners" for the financial support. Y.S. acknowledges the Polish Academy of Sciences for the PAS−NASU Scholarship Program. D.V. acknowledges support from the Research Council of Lithuania (project COLED, No S-MIP-24-2). P.S. gratefully acknowledges Horizon Europe, the European Union's framework programme for research and innovation (R&I) for 2021-2027, project HELIOS, grant agreement No 101155017. The authors gratefully acknowledge Polish high-performance computing infrastructure PLGrid (HPC Centers: ACK Cyfronet AGH, WCSS) for providing computer facilities and support within computational grant no. PLG/2025/018787. We are also sincerely grateful to Dr. Katarzyna Rybicka-Jasińska (Institute of Organic Chemistry PAS) for the help with cyclic voltammetry measurements, to Prof. Daniel T. Gryko and Prof. Agnieszka Szumna (Institute of Organic Chemistry PAS) for permission to use their instruments.

■ ABBREVIATIONS

OLED	organic light emitting diode
EQE	external quantum efficiencies
WOLED	white organic light-emitting diode
BF_2	difluoroboron
DIPEA	diisopropylethylamine
TGA	thermogravimetric analysis
DSC	differential scanning calorimetry
HOMO	highest occupied molecular orbital
LUMO	lowest unoccupied molecular orbital
SOCME	spin-orbit coupling matrix elements
SOC	spin-orbit coupling
S_1	first singlet excited state
T_1	first triplet excited state
TADF	thermally activated delayed fluorescence
T_2	second triplet excited state
CV	cyclic voltammetry
IP	ionization potential
EA	electron affinity
E^{onset}_{ox}	oxidation potential
E^{onset}_{red}	reduction potential
PL	photoluminescence
TD-DFT	time-dependent density functional theory
PLQY	photoluminescence quantum yield
PMMA	polymethylmethacrylate
ITO	indium tin oxide
HATCN	1,4,5,8,9,11-Hexaazatriphenylenehexacarbonitrile
NPB	*N*,*N*′-di(1-naphthyl)-*N*,*N*′-diphenyl-(1,1′-biphenyl)-4,4′-diamine
TCTA	tris(4-carbazoyl-9-ylphenyl)amine
TSPO1	diphenyl[4-(triphenylsilyl)phenyl]phosphine oxide
TPBi	2,2′,2″-(1,3,5-benzenetriyl)tris(1-phenyl-1*H*-benzimidazole)
5TCzBN	2,3,4,5,6-pentakis(3,6-di-tert-butyl-9H-carbazol-9-yl)benzonitrile
CIE	Commission Internationale de l'Éclairage
mCBP	3,3′-di(9*H*-carbazol-9-yl)-1,1′-biphenyl
EL	electroluminescence
RISC	reverse intersystem crossing
FWHM	full width at half-maximum
TLC	thin-layer chromatography
HRMS	high-resolution mass spectra
APCI	atmospheric-pressure chemical ionization
q-TOF	quadrupole-time-of-flight

■ REFERENCES

(1) Hong, G.; Gan, X.; Leonhardt, C.; Zhang, Z.; Seibert, J.; Busch, J. M.; Bräse, S. A Brief History of OLEDs − Emitter Development and Industry Milestones. *Adv. Mater.* **2021**, *33* (9), 2005630.

(2) Cole, C. M.; Yambem, S. D. Thermally Activated Delayed Fluorescent Organic Light Emitting Diodes: Solution Processed to Printed. *Adv. Opt. Mater.* **2025**, *13*, 2402019.

(3) Kang, J.; Shin, D. J.; Lee, J. Y. Recent Advances in Narrow Emission Bandwidth Materials for Application in Organic Light-Emitting Diodes. *Adv. Opt. Mater.* **2025**, *13*, 2402653.

(4) Kim, J.-K.; Kim, B.-S.; Jang, J.-H.; Choi, H.-S.; Ahn, B.-G.; Han, M.-Y.; Sung, C.-J.; Baek, J.-H.; Bae, S.-J.; Shin, W.-S.; Lee, H.-W.; Yoon, S.-Y. The latest milestone in WOLED technology for OLED TV and IT displays: Enhancing efficiency, color gamut, and longevity. *J. Soc. Inf. Display* **2025**, *33* (5), 390−397.

(5) Tian, X.; Xia, Y.; Li, J.; Sun, J.; Wang, H. Recent progress in organic dual-emission materials for white organic light emitting diodes (WOLEDs) from single small-molecule components. *J. Mater. Chem. C* **2025**, *13* (22), 11017−11039.

(6) Fan, C.; Yang, C. Yellow/orange emissive heavy-metal complexes as phosphors in monochromatic and white organic light-emitting devices. *Chem. Soc. Rev.* **2014**, *43* (17), 6439−6469.

(7) Murali, A. C.; Nayak, P.; Venkatasubbaiah, K. Recent advances in the synthesis of luminescent tetra-coordinated boron compounds. *Dalton Trans.* **2022**, *51* (15), 5751−5771.

(8) Brodeur, J.; Hu, L.; Malinge, A.; Eizner, E.; Skene, W. G.; Kéna-Cohen, S. Highly Efficient and Spectrally Narrow Near-Infrared Fluorescent OLEDs Using a TADF-Sensitized Cyanine Dye. *Adv. Opt. Mater.* **2019**, *7* (22), 1901144.

(9) Kutsiy, S.; Volyniuk, D.; Sahoo, S. R.; Ceborska, M.; Wisniewska, A.; Stakhira, P.; Grazulevicius, J. V.; Baryshnikov, G. V.; Potopnyk, M. A. Sterically Tuned *Ortho*-Phenylene-Linked Donor−Acceptor Benzothiazole-Based Boron Difluoride Complexes as Thermally-

https://doi.org/10.1021/acsaelm.6c00557
ACS Appl. Electron. Mater. 2026, 8, 5372−5383

Activated Delayed Fluorescence Emitters for Organic Light-Emitting Diodes. *ACS Appl. Mater. Interfaces* **2024**, *16* (44), 60633−60647.
(10) Kutsiy, S.; Bezvikonnyi, O.; Hotynchan, A.; Volyniuk, D.; Luboradzki, R.; Zinchenko, H. M.; Wisniewska, A.; Stakhira, P.; Grazulevicius, J. V.; Potopnyk, M. A. Donor−Acceptor Boron Difluoride Complexes for Bipolar Exciplex Emitters in Organic Light-Emitting Diodes. *ACS Appl. Mater. Interfaces* **2025**, *17* (44), 60956−60968.
(11) Zinchenko, H. M.; Ivaniuk, K.; Hotynchan, A.; Jean-Woldemar, E.; Marek-Urban, P. H.; Mech-Piskorz, J.; Ceborska, M.; Pander, P.; Kędra, K.; Chénais, S.; Angulo, G.; Durka, K.; Forget, S.; Potopnyk, M. A. Donor−Acceptor Benzochalcogenazolo-Based *N,O*-Coordinated Boron Difluoride Emitters Exhibiting Amplified Spontaneous Emission and Thermally Activated Delayed Fluorescence for Organic Light-Emitting Diodes. *ACS Appl. Mater. Interfaces* **2025**, *17* (52), 70722−70739.
(12) Aoki, R.; Komatsu, R.; Goushi, K.; Mamada, M.; Ko, S. Y.; Wu, J. W.; Placide, V.; D'Aléo, A.; Adachi, C. Realizing Near-Infrared Laser Dyes through a Shift in Excited-State Absorption. *Adv. Opt. Mater.* **2021**, *9*, 2001947.
(13) Li, S.; Chen, J.; Wei, Y.; De, J.; Geng, H.; Liao, Q.; Chen, R.; Fu, H. An Organic Laser Based on Thermally Activated Delayed Fluorescence with Aggregation-Induced Emission and Local Excited State Characteristics. *Angew. Chem., Int. Ed.* **2022**, *61*, e202209211.
(14) Pytlarz, R.; Kutsiy, S.; Hotynchan, A.; Jean-Woldemar, E.; Luboradzki, R.; Marek-Urban, P. H.; Merklin, G.; Chénais, S.; Volyniuk, D.; Grazulevicius, J. V.; Durka, K.; Forget, S.; Potopnyk, M. A. Benzochalcogenazolo-based *N,O*-coordinated boron difluoride complexes as gain media for organic solid-state lasers. *J. Mater. Chem. C* **2025**, *13* (32), 16478−16488.
(15) Kong, L.; Huang, Z.; Zhang, S.-S.; Song, J.; Zhang, Y.-Y.; Bai, X.-Y.; Yang, J.-X.; Li, L. A facile strategy to realize a single/double photon excitation-dependent photosensitizer for imaging-guided phototherapy against HeLa cancer cells at separate irradiation channels. *Chem. Commun.* **2020**, *56*, 571−574.
(16) Ashoka, A. H.; Ashokkumar, P.; Kovtun, Y. P.; Klymchenko, A. S. Solvatochromic Near-Infrared Probe for Polarity Mapping of Biomembranes and Lipid Droplets in Cells under Stress. *J. Phys. Chem. Lett.* **2019**, *10* (10), 2414−2421.
(17) Paisley, N. R.; Halldorson, S. V.; Tran, M. V.; Gupta, R.; Kamal, S.; Algar, W. R.; Hudson, Z. M. Near-Infrared-Emitting Boron-Difluoride-Curcuminoid-Based Polymers Exhibiting Thermally Activated Delayed Fluorescence as Biological Imaging Probes. *Angew. Chem., Int. Ed.* **2021**, *60* (34), 18630−18638.
(18) Maeda, H.; Nishimura, T.; Haketa, Y.; Tanaka, H.; Fujita, M.; Yasuda, N. Ion-Pairing Assemblies of Anion-Responsive π-Electronic Systems Bearing Triazole Moieties Introduced by Click Chemistry. *J. Org. Chem.* **2022**, *87* (12), 7818−7825.
(19) Xia, Q.; Yang, J.; Zhang, S.; Zhang, J.; Li, Z.; Wang, J.; Chen, X. Bodipy-Based Metal−Organic Frameworks Transformed in Solid States from 1D Chains to 2D Layer Structures as Efficient Visible Light Heterogeneous Photocatalysts for Forging C−B and C−C Bonds. *J. Am. Chem. Soc.* **2023**, *145* (11), 6123−6134.
(20) Zhao, M.; Ren, F.; Zhou, Y. Construction of Boron Difluoride Complexes with Asymmetric *N,N'*-Bidentate Ligands. *Chem. –Eur. J.* **2024**, *30*, e202401784.
(21) Dhayalan, V.; Dodke, V. S.; Kumar, M. P.; Korkmaz, H. S.; Hoffmann-Röder, A.; Amaladass, P.; Dandela, R.; Dhanusuraman, R.; Knochel, P. Recent synthetic strategies for the functionalization of fused bicyclic heteroaromatics using organo-Li, -Mg and -Zn reagents. *Chem. Soc. Rev.* **2024**, *53* (22), 11045−11099.
(22) Oner, S.; Bryce, M. R. A review of fused-ring carbazole derivatives as emitter and/or host materials in organic light emitting diode (OLED) applications. *Mater. Chem. Front.* **2023**, *7* (19), 4304−4338.
(23) Elgadi, S. A.; Mikulin, S.; Hudson, Z. M. Recent Progress in Organic TADF Emitters Containing Heavy Atoms. *Adv. Opt. Mater.* **2025**, *13* (21), 2500683.
(24) Chen, H.; Deng, Y.; Zhu, X.; Wang, L.; Lv, L.; Wu, X.; Li, Z.; Shi, Q.; Peng, A.; Peng, Q.; Shuai, Z.; Zhao, Z.; Chen, H.; Huang, H. Toward Achieving Single-Molecule White Electroluminescence from Dual Emission of Fluorescence and Phosphorescence. *Chem. Mater.* **2020**, *32* (9), 4038−4044.
(25) Cheng, C.; Gao, N.; Yu, C.; Wang, Z.; Wang, J.; Hao, E.; Wei, Y.; Mu, X.; Tian, Y.; Ran, C.; Jiao, L. Diversity-Oriented Facile Access to Highly Fluorescent Membran-Permeable Benz[*c,d*]indole *N*-Heteroarene BF_2 Dyes. *Org. Lett.* **2015**, *17* (2), 278−281.
(26) Shimizu, S.; Murayama, A.; Haruyama, T.; Iino, T.; Mori, S.; Furuta, H.; Kobayashi, N. Benzo[*c,d*]indole-Containing Aza-BODIPY Dyes: Asymmetrization-Induced Solid-State Emission and Aggregation-Induced Emission Enhancement as New Properties of a Well-Known Chromophore. *Chem. –Eur. J.* **2015**, *21* (7), 12996−13003.
(27) Kutsiy, S.; Pytlarz, R.; Hotynchan, A.; Marek-Urban, P. H.; Luboradzki, R.; Jean-Woldemar, E.; Volyniuk, D.; Chénais, S.; Forget, S.; Durka, K.; Grazulevicius, J. V.; Potopnyk, M. A. Chalcogen-Influenced Benzochalcogenazolo-Based *N,O*-Coordinated Difluoroboron Complexes: From Lasing Dyes to Room-Temperature-Phosphorescence Emitters. *Inorg. Chem.* **2025**, *64* (28), 14704−14716.
(28) Göbel, D.; Rusch, P.; Duvinage, D.; Bigall, N. C.; Nachtsheim, B. J. Emission color-tunable oxazol(in)yl-substituted excited-state intramolecular proton transfer (ESIPT)-based luminophores. *Chem. Commun.* **2020**, *56* (98), 15430−15433.
(29) Zhang, D.; Cai, M.; Zhang, Y.; Zhang, D.; Duan, L. Sterically shielded blue thermally activated delayed fluorescence emitters with improved efficiency and stability. *Mater. Horiz.* **2016**, *3* (2), 145−151.
(30) Gottlieb, H. E.; Kotlyar, V.; Nudelman, A. NMR Chemical Shifts of Common Laboratory Solvents as Trace Impurities. *J. Org. Chem.* **1997**, *62* (21), 7512−7515.
(31) Frisch, M. J.; Trucks, G. W.; Schlegel, H. B.; Scuseria, G. E.; Robb, M. A.; Cheeseman, J. R.; Scalmani, G.; Barone, V.; Petersson, G. A.; Nakatsuji, H.; Li, X.; Caricato, M.; Marenich, A. V.; Bloino, J.; Janesko, B. G.; Gomperts, R.; Mennucci, B.; Hratchian, H. P.; Ortiz, J. V.; Izmaylov, A. F.; Sonnenberg, J. L.; Williams-Young, D.; Ding, F.; Lipparini, F.; Egidi, F.; Goings, J.; Peng, B.; Petrone, A.; Henderson, T.; Ranasinghe, D.; Zakrzewski, V. G.; Gao, J.; Rega, N.; Zheng, G.; Liang, W.; Hada, M.; Ehara, M.; Toyota, K.; Fukuda, R.; Hasegawa, J.; Ishida, M.; Nakajima, T.; Honda, Y.; Kitao, O.; Nakai, H.; Vreven, T.; Throssell, K.; Montgomery, Jr.J. A.; Peralta, J. E.; Ogliaro, F.; Bearpark, M. J.; Heyd, J. J.; Brothers, E. N.; Kudin, K. N.; Staroverov, V. N.; Keith, T. A.; Kobayashi, R.; Normand, J.; Raghavachari, K.; Rendell, A. P.; Burant, J. C.; Iyengar, S. S.; Tomasi, J.; Cossi, M.; Millam, J. M.; Klene, M.; Adamo, C.; Cammi, R.; Ochterski, J. W.; Martin, R. L.; Morokuma, K.; Farkas, O.; Foresman, J. B.; Fox, D. J. *Gaussian 16*; Gaussian, Inc.: Wallingford CT, **2016**.
(32) Andrae, D.; Haeussermann, U.; Dolg, M.; Stoll, H.; Preuss, H. Energy-adjusted ab initio pseudopotentials for the second and third row transition elements. *Theor. Chim. Acta* **1990**, *77* (2), 123−141.
(33) Lewis, J. E. M.; Tarzia, A.; White, A. J. P.; Jelfs, K. E. Conformational control of Pd2L4 assemblies with unsymmetrical ligands. *Chem. Sci.* **2020**, *11* (3), 677−683.
(34) Dennington, R.; Keith, T. A.; Millam, J. M.In: *GaussView, Version 6*; Semichem Inc.: Shawnee Mission, KS, **2016**.

https://doi.org/10.1021/acsaelm.6c00557
ACS Appl. Electron. Mater. 2026, 8, 5372−5383